

meridional secondary flow [5,6].

' "8 YgW]dHcb' cZH Y'a cXY'

The object of the investigation is a modified Rayleigh-Bénard configuration, a cylindrical melt column of variable aspect ratio homogeneously heated from below. The photo in Fig. 1 illustrates the experimental setup mounted inside the magnetic coil system MULTIMAG [7]. Besides the already mentioned RMF, it offers a variety of other magnetic field types, such as the traveling (TMF), pulsed (PMF), vertical DC or vertical DC of cusp type, and even linear superposition thereof. As working fluid the ternary alloy GaInSn [8] was used because it remains liquid at room temperature and as distinguished from mercury it is non-poisonous. Moreover, its low Prandtl number is similar to that of molten silicon.

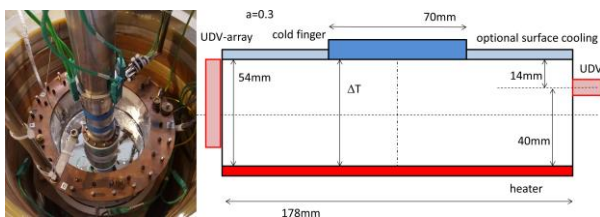


Figure 1: View to the experimental setup mounted inside the coil system on the left side. Some geometrical parameters are indicated in the schema on the right side.

The heating was realized by an electrical heating plate embedded in a massive copper disc to achieve isothermal boundary conditions. Several thermocouples were installed inside the copper disc to monitor its temperature. The upper thermal boundary condition in a Cz system is realized by a partially cooled surface. The partial cooling in our experiment covers approximately the same fraction area as the crystal does in an industrial facility. It is realized with a circular heat exchanger (cold finger) mounted concentrically at the top of the experimental cell. The cold finger is optionally rotatable, a precise control of the temperature is realized by supplying it with coolant fluid at high flow rate from a thermostat having a large reservoir. The temperature of the cold finger is also monitored at various positions. During the measurements, the apparatus was embedded in mineral wool to minimize the lateral heat loss.

Flow velocities were measured by the UDV technique, the principle of operation is described in the pioneering work by Takeda [9]. Mainly two features render UDV predestinated for the present work. Firstly, it works in opaque media including liquid metals. Secondly, it allows the quasi-simultaneous measurement of an entire profile of the local velocity component in direction of the sound propagation along the ultrasonic beam.

Two different sensor arrangements were used which are shown in Fig. 2. Most of the measurements were taken by a DOP2000 velocimeter (Signal-Processing, Lausanne, Switzerland) with single ultrasound transducers. As it can be seen on the left side of Fig. 2 six single sensors were arranged at different azimuthal positions, each one differing by 30° to the next one. This allows gathering flow

information over the whole circumference of the vessel. Furthermore, the different mounting levels allow measurements for variable aspect ratios.



Figure 2: View to the instrumentation for the flow measurements. On the left side the option with single transducers and on the right with the ultrasound array. The single transducers are coupled through holes directly to the melt whereas the UDV array measures through the wall of 2.3 mm thickness.

The right side in Fig. 2 shows a second setup with an attached transducer array. The reason for this setup was of preliminary character to check and qualify the UDV array technique for a more complex setup in the near future. The UDV array consists of 25 single transducer elements arranged linearly, each of a size of 2.3×5 mm² with an element pitch of 2.7 mm. Thus, it allows flow measurements of the velocity component perpendicular to the transducer surface over a field width of 67 mm. Moreover, multiple array arrangements would allow measurements of more velocity components and therefore complex flow mapping in the covered plane. For details on the UDV array technique [10,11] are referred to.

(' "FYgi `tg'

For the present study flow velocity measurements were performed at mainly two different aspect ratios, $a = 0.45$ ($H = 80$ mm) and $a = 0.3$ ($H = 54$ mm), and under the influence of different types of magnetic fields (RMF, TMF, cusp). Nevertheless, only a small cutout of some selected aspects can be presented in this paper.

In the range $1.4 \times 10^6 \leq Gr \leq 1.6 \times 10^8$ two different flow regimes were identified and investigated for $a = 0.3$. The vertical position of the sensors was thereby at $h = 40$ mm. For a low temperature gradient of $\Delta T = 1$ K ($Gr = 1.6 \times 10^6$) an axisymmetric flow structure occurs. The fluid heated from the bottom rises along the rim, continues towards the center axis, drops in the central region below the cold finger and closes outward to the rim. Fig. 3 on the left illustrates such a measurement done with one single transducer at the randomly selected azimuthal position $\varphi = 0^\circ$. Already for slightly higher $\Delta T = 3.1$ K ($Gr = 5.1 \times 10^6$) the axisymmetric flow topology becomes unstable (cf. Fig. 3-right) and for further increased Gr ($Gr = 4.2 \times 10^7$, $\Delta T = 22$ K) the flow develops the wind structure which is a large scale single roll circulating inside the vessel. Such a structure is well-known in general RB systems and frequently observed for $a = 1.0$.

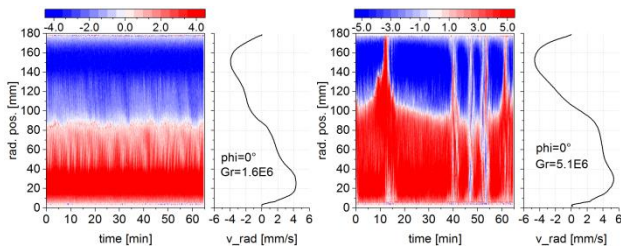


Figure 3: Left: time series and the related mean profile of the radial velocity component measured at $\varphi = 0^\circ$ in the axisymmetric case. Right: typical velocity signal in the transitional range. In both cases, similar diagrams result at the other azimuthal positions φ .

It should be mentioned here that the preferred main flow direction of the wind develops randomly and is influenced mainly from the circumstances of the experimental setup. Fig. 4 shows two time series measurements in the wind-mode at the positions $\varphi = 0^\circ$ and $\varphi = 90^\circ$. The latter one corresponds thereby to the main circulation loop of the flow.

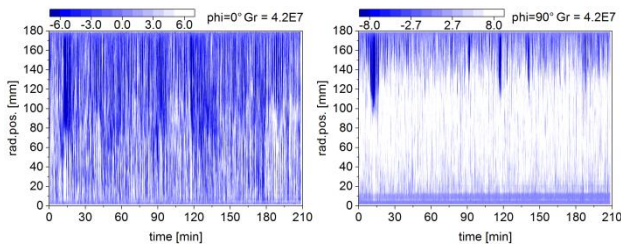


Figure 4: Time series observed for long term measurements in the wind-mode. The velocity units are given in mm/s.

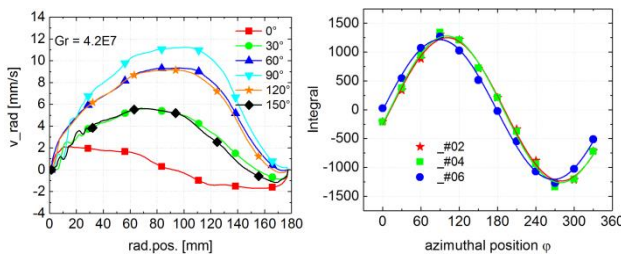


Figure 5: Left: Mean radial velocity profiles across the diameter for the wind-mode. Right: typical surface integrals of the mean profiles for different measurements.

The orientation of the wind becomes clearer from Fig. 5 where the left diagram shows the mean radial velocity profiles at each of the azimuthal positions and the right one surface integral of the respective profile. The maximum in the curve at approximately $\varphi = 90^\circ$ indicates therewith clearly the main circulation loop of the wind. Furthermore, the right part of Fig. 5 summarizes three different measurements performed at different days and demonstrates well the stability of the wind. At the same time it can be mentioned, that this was not the case for $a = 0.45$. Although here not shown, the wind was in that sense unstable, that the maximum of the integral curves varied in time over a large azimuthal range, even flow reversals were occasionally observed.

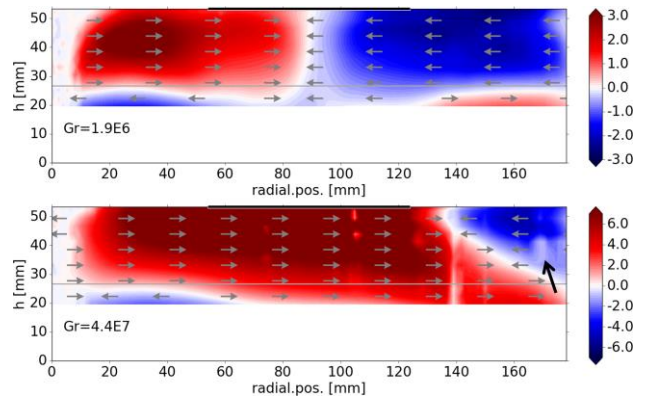


Figure 6: Radial flow maps measured using the UDV array. Arrows indicate only the flow direction and are not scaled. Due to construction reasons the lower 20 mm could not be measured. Since the array measures through the wall of the vessel, the quality of the signal is significantly influenced by the ultrasonic coupling both at the inner and outer interface of the wall. In “suboptimal” cases stationary echoes may occur which appear as “abnormal spots” in the flow map (also present in the above diagram marked with the thick black arrow). The velocity units are given in mm/s.

As mentioned in section 3, some selected measurements were done by means of the UDV array in a second setup. Due to the ability to measure quasi simultaneously along several sensor lines, a more informative radial flow map is achieved. Fig. 6 shows in the upper diagram such a purely buoyancy driven radial flow map in the axisymmetric low Gr case and for the fully developed wind-mode in the lower part. Furthermore, it is obvious from the lower diagram that the azimuthal position of the UDV array does not corresponds fully with the main circulation loop of the flow, which is again a consequence of the random character of the wind.

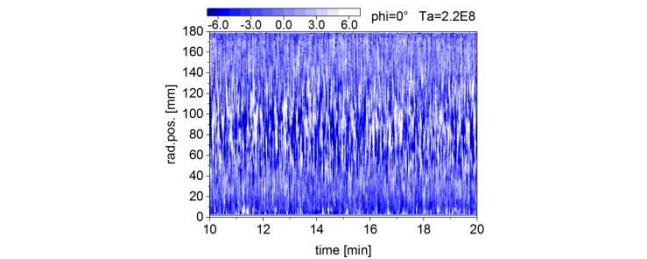
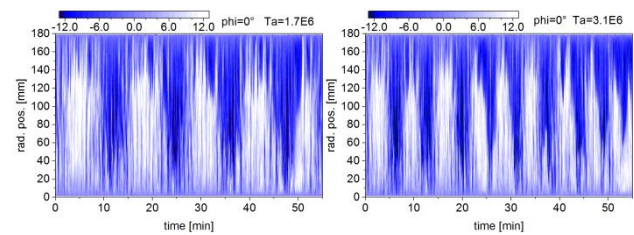


Figure 7: Influence of the RMF on the wind-mode ($Gr = 4.5 \times 10^7$). In the upper part time series of the radial flow measured at $\varphi = 0^\circ$ for two different, relatively low strengths of the RMF. The lower diagram shows the case for a strong RMF. The velocity units are given in mm/s.

Applying an increasing RMF to the wind-mode it causes in the first instance a co-rotation of the wind as well - cf.

upper part of Fig. 7. For a high enough Ta the wind completely disappears (see in the lower diagram of Fig. 7).

A different influence of the RMF is observed by applying it to the axisymmetric case. The diagrams in Fig. 8 visualize the single sensor measurements for three different Ta numbers. At first glance, common to the diagrams are the first few minutes in which the RMF was not yet switched on. The axisymmetric structure is clearly observed here. When the RMF is switched on, some minor differences are observed between $Ta = 1.0 \times 10^6$ and $Ta = 1.4 \times 10^6$. For $Ta = 2.6 \times 10^6$ the axial symmetry disappears, rather a similarity to the wind structure is observed – at least along the single sensor measurement line ($h = 40$ mm).

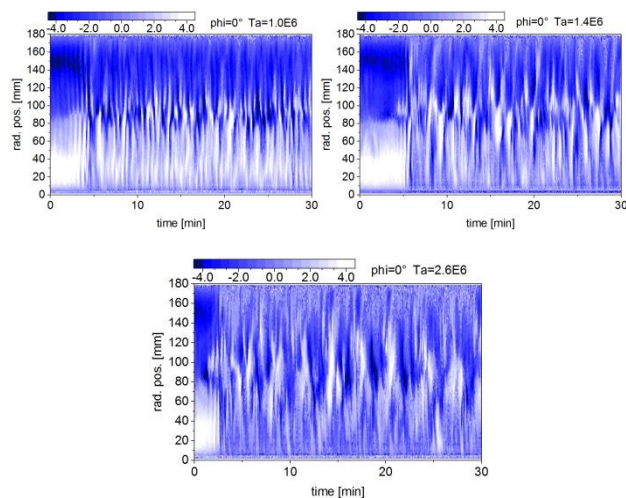


Figure 8: The flow under the influence of different RMFs in the axisymmetric case with $Gr = 1.6 \times 10^6$. The velocity units are given in mm/s.

Of course it might be somewhat misleading to conclude from a one line measurement to the overall flow structure. In this regard, the major feature of the UDV array to measure simultaneously several lines becomes rather advantageous. The diagrams in Fig. 9 illustrate the mean radial flow maps for the same Gr and Ta numbers as specified in Fig. 8. By increasing the RMF strength rather a kind of squeezing occurs and the inward flow at the upper part of the vessel concentrates more and more to the region below the surface. Since the diagrams in Fig. 9 are the result of an averaging process over the measuring time of about 1 hour, the flow still has a time dependent and complex behaviour. Thus, care has to be taken by interpreting the overall flow topology.

) "Gi a a Ufm

A Cz-like crystal growth model exposed to different magnetic fields was the object of the present investigation. Ultrasound measurements of the fluid flow were performed by varying the strength of the RMF (Ta) and that of the buoyancy (Gr). Besides the single ultrasound transducers, the UDV array, whenever applicable to the specific setup, might provide a deeper insight into the complex flow topology in a Cz setup. Furthermore, the experimental data here serve as a benchmark object for

numerical codes which are still under development.

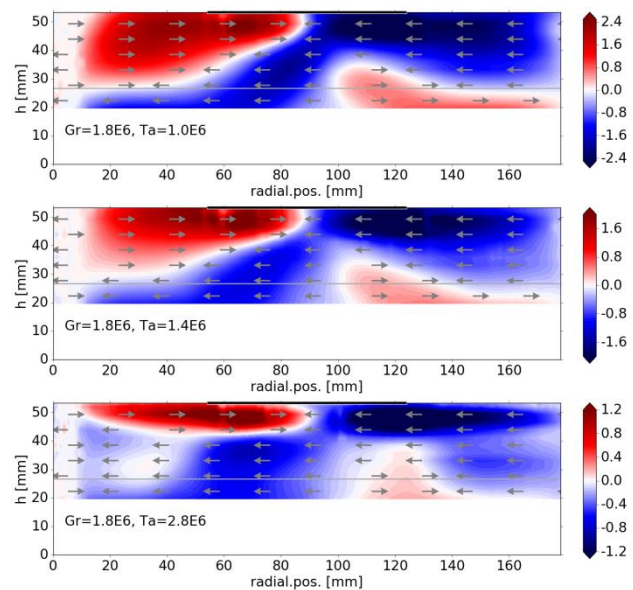


Figure 9: Mean radial flow maps under the same conditions as indicated in Fig. 8. The velocity units are given in mm/s.

* "5 W_bck `YX[Ya Yblg`

Financial support by the Federal Ministry for Economic Affairs and Energy in the framework of the KORONA project is gratefully acknowledged.

F YZ/fYbWwG`

- [1] J. Czochralski: Ein neues Verfahren zur Messung der Kristallisationsgeschwindigkeit der Metalle (in german), *Z. Physik. Chem.* 92 (1917), 219–221.
- [2] K. Kakimoto, *et al.*: Review. Growth of semiconductor silicon crystals, *Progress in Crystal Growth and Characterization of Materials* 62 (2016), 273–285.
- [3] F. Hébert, *et al.*: Onset of Rayleigh-Bénard convection in cylindrical containers, *Phys. Rev. E* 81 (2001), 046318.
- [4] J. Niemela, *et al.*: The wind in confined thermal convection, *J. Fluid Mech.* 449 (2001), 169–178.
- [5] L.P. Gorbatchev, *et al.*: Magnetohydrodynamic rotation of an electrically conductive liquid in a cylindrical vessel of finite dimensions, *Magnetohydrodynamics* 10 (1974), 406–414.
- [6] P.A. Davidson: Swirling flow in an axisymmetric cavity of arbitrary profile driven by a rotating magnetic field, *J. Fluid Mech.* 245 (1992), 669–699.
- [7] J. Pal *et al.*: MULTIMAG - A MULTIpurpose MAGNetic system for physical modelling in magnetohydrodynamics, *Flow. Meas. Instrum.*, 20 (2009), 241–251.
- [8] Y. Plevachuk, *et al.*: Thermophysical Properties of the Liquid Ga–In–Sn Eutectic Alloy, *J. Chem. Eng. Data* 59(3) (2014), 757–763.
- [9] Y. Takeda: Development of an ultrasound velocity profile monitor, *Nucl. Eng. Des.* 126 (1991), 277–284.
- [10] S. Franke *et al.*: 2d-2c Ultrasound Doppler Array Velocimeter for Flow Investigations in Liquid Metals, *Proceedings of ISUD7 Gothenburg/Sweden*, (2010), 89–92.
- [11] S. Franke *et al.*: Two-dimensional ultrasound Doppler velocimeter for flow mapping of unsteady liquid metal flows, *Ultrasonics* 53 (2013), 691–700.